Meteorology and Atmospheric Physics (2022) 134:78
https://doi.org/10.1007/s00703-022-00913-6

ORIGINAL PAPER

Trends and variabilities of precipitation and temperature extremes over Southeast Asia during 1981–2017

Yi Fan[1] · Jiayao Li[1] · Shoupeng Zhu[2] · Huixin Li[1] · Botao Zhou[1]

Received: 31 August 2021 / Accepted: 29 June 2022 / Published online: 28 July 2022

Abstract
As one of the most populated agricultural habitats in the world, Southeast Asia has been highly exposed to extremes of weather and climate, posing great importance to figure out the trend and variability characteristics of extremes over there. The annual extreme precipitation and temperature over Southeast Asia during 1981–2017 are analyzed in this study using datasets based on daily observations derived from thousands of meteorological stations. Results show that the wet extremes decrease over the areas surrounding the South China Sea and increase over the south of the Philippines and Indonesia with the most significant trends detected over the east of Indochina and New Guinea. Extreme high temperatures decrease significantly over the middle of New Guinea and increase over Indochina, Sumatra, Java, and Kalimantan. Moreover, empirical orthogonal function (EOF) analyses show that the first principal components for most precipitation extremes are characterized by significant decadal changes relevant to the Atlantic Multidecadal Oscillation and Pacific Decadal Oscillation, and the second principal components exhibit significant interannual variability associated with oceanic systems such as El Niño–Southern Oscillation (ENSO). As for temperature extremes, the leading EOF modes show non-significant trends or decadal variations, but significant interannual variations related to ENSO and the Indian Ocean Dipole are detected.

1 Introduction

Since the 1950s, due to rapidly increasing concentrations of greenhouse gases (Brohan et al. 2006; IPCC 2013), the warming world has led to rising sea levels, shrinking snow and ice covers, inducing variations in the trends, frequency, and intensity of climate extremes globally (Alexander et al. 2006; Fan et al. 2014; Fischer and Knutti 2015; Schleussner et al. 2016). These extremes include extraordinary temperature and precipitation, which have never been evenly distributed for either temporal or spatial aspects (Donat et al. 2013).

Southeast Asia, consisting of Indochina and the Malay Archipelago, is a key area connecting Asia with the Indian Ocean and the Pacific Ocean. Being densely populated and highly agriculture-reliant, the lives and economies over Southeast Asia are under great impacts of both precipitation and temperature extremes (Zander et al. 2019). Projections on the future under different global warming levels show that the most obvious extreme changes would predominantly occur in the coastal areas, and higher global warmings are more likely to induce stronger extremes (Manton et al. 2001; Endo et al. 2009; Caesar et al. 2011; Zhu et al. 2020). So far, previous studies have mostly concentrated on how the Southeast Asia climate extremes change in the future, while the trends and variabilities during the recent decades have not yet been comprehensively investigated.

It is widely known that variability of the Asian climate is profoundly impacted by internal variability of oceanic systems such as the Atlantic Multidecadal Oscillation (AMO), Pacific Decadal Oscillation (PDO), El Niño–Southern Oscillation (ENSO), and Indian Ocean Dipole (IOD) (Nicholls et al. 2005; Della-Marta et al. 2007; Si and Ding 2016; Thirumalai et al. 2017; Cheong et al. 2018; Li and Yuan 2019; Qian and Zhang 2019). ENSO and IOD are two important modes over the Pacific and the Indian Ocean,

Responsible Editor: Stephanie Fiedler.

✉ Yi Fan
fanyi@nuist.edu.cn

[1] Collaborative Innovation Center on Forecast and Evaluation of Meteorological Disasters (CIC-FEMD)/Key Laboratory of Meteorological Disaster, Ministry of Education/School of Atmospheric Sciences, Nanjing University of Information Science and Technology, Nanjing 210044, China

[2] Key Laboratory of Transportation Meteorology of China Meteorological Administration, Nanjing Joint Institute for Atmospheric Sciences, Nanjing 210041, China

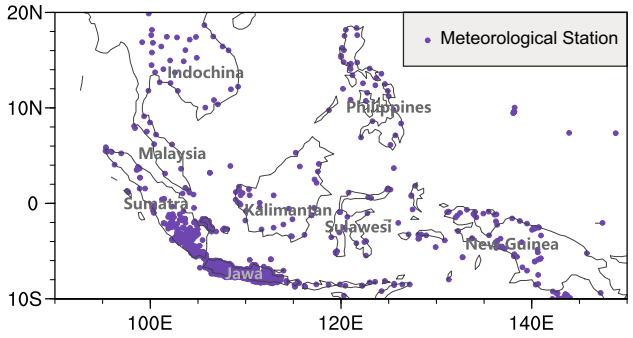

Fig. 1 The study area and spatial distribution of meteorological stations

respectively, modulating variations of the temperature and precipitation anomalies over Southeast Asia mainly through exciting anomalous circulations over the western North Pacific (Thirumalai et al. 2017; Cheong et al. 2018; Fan et al. 2019). Moreover, changes of the AMO and PDO are demonstrated to modulate the South China Sea summer monsoon and summer precipitation over Southern China via modulating ENSO variability and propagation path of mid-high-latitude Rossby wave activities (Zhou and Wu 2016; Fan and Fan 2017; Fan et al. 2019). Notably, whether these natural variabilities emerge significant modifications in extreme climates over Southeast Asia remains unclear. Therefore, the relationships between these large-scale atmosphere–ocean systems and the extremes of precipitation and temperature over Southeast Asia are to be explored in this study.

The article is organized as follows. The data and methods are briefly described in Sect. 2. Section 3 provides the spatial and temporal characteristics of temperature and precipitation extremes over Southeast Asia. In Sect. 4, the general relationships between the extremes and oceanic factors such as the AMO, PDO, ENSO, and IOD are investigated. Finally, the conclusion and discussion are given in Sect. 5.

2 Data and methods

Observations of daily temperature and precipitation over Southeast Asia for the period of 1981–2017 are provided by the Southeast Asia Climate Assessment and Dataset project with a horizontal resolution of 0.5° × 0.5°, which are referred to as the SA-OBSv2.0 dataset (van den Besselaar et al. 2017; Ge et al. 2021). This dataset is derived, with the qualities strictly controlled, from the observations of meteorological stations (Fig. 1).

Monthly Sea Surface Temperature (SST) data are the Extended Reconstructed SST V5 provided by the U.S. National Oceanic and Atmospheric Administration with a horizontal resolution of 2° × 2° during 1981–2017 (Huang et al. 2017). Geopotential height and wind datasets are obtained from the European Centre for Medium-Range Weather Forecasts (ECMWF) ERA5 with a horizontal resolution of 0.25° × 0.25° (Hersbach et al. 2019).

Following the recommendations of the Expert Team on Climate Change Detection and Indices (ETCCDI), 11 indices quantitatively describing temperature and precipitation extremes are listed in Table 1. More details can be found at the ETCCDI website (http://etccdi.pacificclimate.org/indices.shtml). In addition, the monthly series of the AMO index, the PDO index, the ENSO Index, and the IOD index are obtained from the U.S. National Oceanic and Atmospheric Administration Physical Sciences Laboratory (https://psl.noaa.gov). The AMO index is calculated by averaged SST anomalies in the Atlantic north of the equator. PDO is obtained through the leading principal component of monthly SST anomalies in the North Pacific Ocean (poleward of 20° N). ENSO is monitored using the Niño 3.4 SST index which is the average SST anomalies over east-central Tropical Pacific SST (5° S–5° N and 170°–120° W). The IOD is represented with the dipole mode index (DMI) which is the difference of the area mean SST anomalies in

Table 1 Definitions of extreme indices

ID	Index name	Definitions	Units
SDII	Daily precipitation intensity	Total precipitation divided by the number of wet days (PRCP ≥ 1 mm)	mm/day
R10mm	Number of heavy precipitation days	Number of days when PRCP ≥ 10 mm/year	days
R20mm	Number of very heavy precipitation days	Number of days when PRCP ≥ 20 mm/year	days
RX5day	Maximum 5-day precipitation	Maximum consecutive 5-day precipitation per year	mm
CDD	Consecutive dry days	Maximum number of consecutive days with daily precipitation < 1 mm/year	days
CWD	Consecutive wet days	Maximum number of consecutive days with daily precipitation ≥ 1 mm/year	days
TXx	Maximum of daily maximum temperature	The maximum value of daily maximum temperature per year	°C
TNx	Maximum of daily minimum temperature	The maximum value of daily minimum temperature per year	°C
TXn	Minimum of daily maximum temperature	The minimum value of daily maximum temperature per year	°C
TNn	Minimum of daily minimum temperature	The minimum value of daily minimum temperature per year	°C
DTR	Daily temperature range	The difference between daily maximum and minimum temperature per year	°C

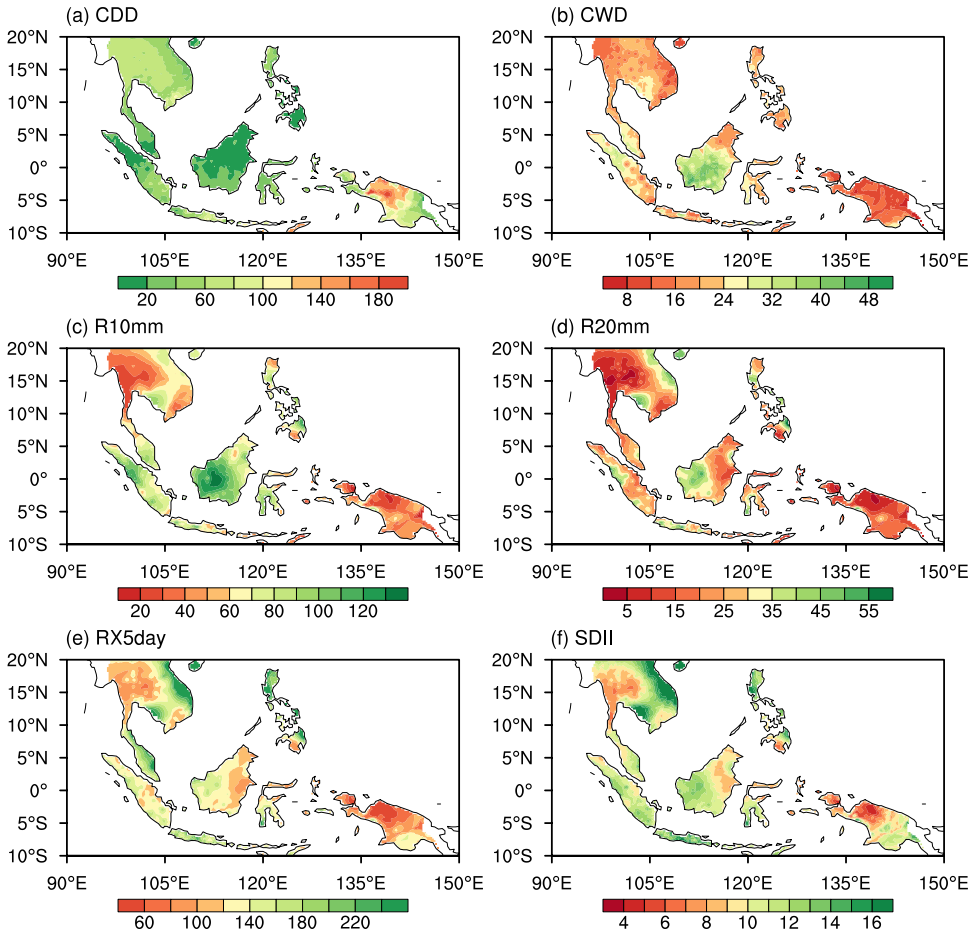

Fig. 2 Spatial distributions of the climatological mean **a** CDD, **b** CWD, **c** R10mm, **d** R20mm, **e** RX5day, and **f** SDII over Southeast Asia during 1981–2017

the western equatorial Indian Ocean (W-IO) (50°–70° E and 10° S–10° N) and the southeastern equatorial Indian Ocean (E-IO) (90°–110° E and 10° S–0°).

Aiming at investigating the spatial and temporal variation characteristics of the precipitation and temperature extremes over Southeast Asia, the Empirical Orthogonal Function (EOF) analysis is employed, which is a method analyzing the structural characteristics of matrix data and is widely used in climate-related studies. The running *t* test is utilized to detect the decadal variation of extreme temperature and precipitation. The trends of the extreme indices from 1981 to 2017 are calculated by simple linear regression. Pearson correlation coefficients between extremes indices and the typical ocean systems are calculated to analyze the possible underlying influences of oceanic factors on extremes in Southeast Asia.

3 Results

3.1 Precipitation extremes

3.1.1 Climatological means

Spatial distributions of the climatological means of extreme precipitation indices over Southeast Asia during 1981–2017 are shown in Fig. 2. It is indicated that New Guinea and western Indochina are characterized by generally more intense drought extremes than Kalimantan and eastern Indochina. The consecutive dry days (CDD) are lower than 60 days over Malaysia, Kalimantan, the southern Philippines, and northern Sumatra, while greater than 100 days over central New Guinea indicating its longer range of dry season (Fig. 2a). On the other hand, it shows higher consecutive wet days (CWD) values over Kalimantan and relatively lower over most areas of New Guinea (Fig. 2b). The number of heavy precipitation days (R10mm) values is greater than 60 days over Kalimantan, the center of the Philippines, and some parts of Sumatra, while less than 60 days over western Indochina and New Guinea (Fig. 2c). Meanwhile, the number of very heavy precipitation days (R20mm) (Fig. 2d)

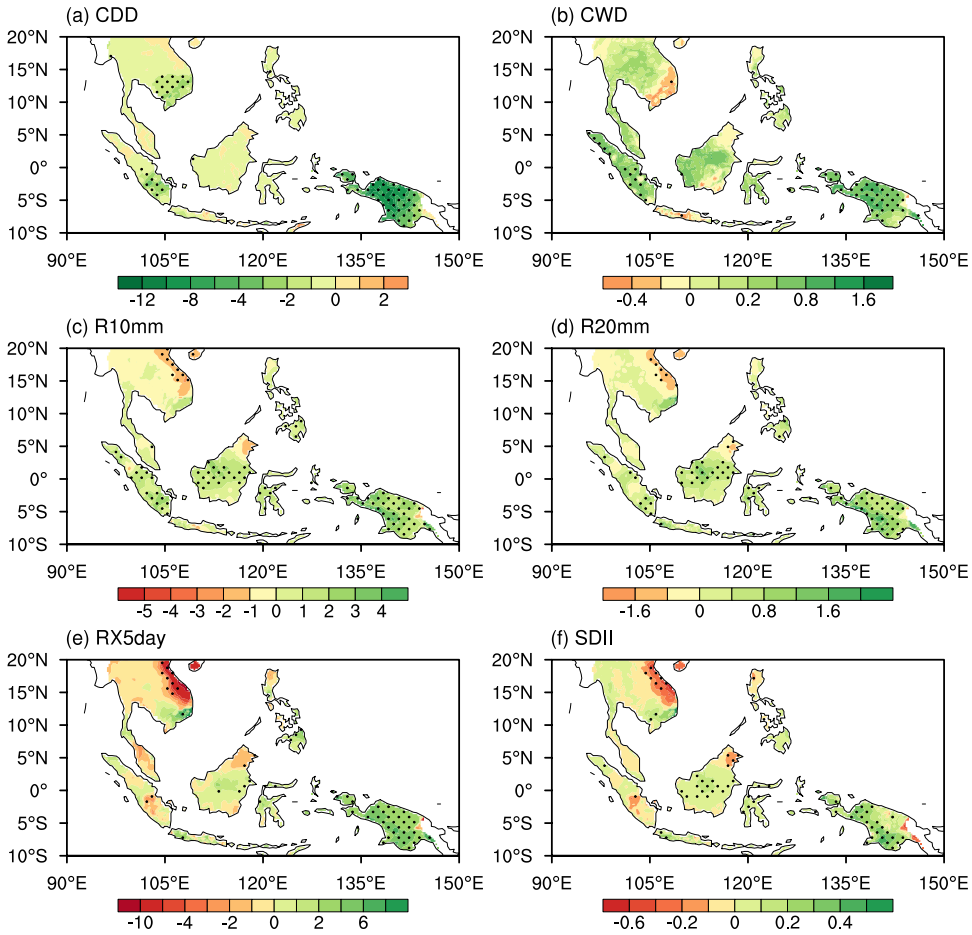

Fig. 3 Spatial distributions of the linear trends of **a** CDD, **b** CWD, **c** R10mm, **d** R20mm, **e** RX5day, and **f** SDII over Southeast Asia during 1981–2017. Dotted areas are significant at the 0.01 significance level according to the Student's *t* test

and the daily precipitation intensity (SDII) (Fig. 2f) both show similar spatial distribution patterns to the R10mm. The maximum 5-day precipitations (RX5day) greater than 160 mm are mainly located over northeastern Indochina, the western of Malaysia, and the northern Philippines (Fig. 2e), and those lower than 140 mm are over most areas in western Indochina, Indonesia, the eastern of Malaysia, and New Guinea.

3.1.2 Trends

The linear trend distributions of precipitation extremes over Southeast Asia during 1981–2017 represented by the coefficients of extremes indices regression on time are displayed in Fig. 3. The CDD shows a significantly decreasing trend at a rate of 0–4.0 over southern Indochina and the middle of Sumatra. In addition, more conspicuous decrease can be detected over New Guinea by 4.0–12.0 (Fig. 3a). In contrast, the CWD slightly increases over almost the whole area, with significant trends mainly distributed over Sumatra and New Guinea (Fig. 3b). The R10mm increases by 0–3.0 over Indochina, northern Malaysia, and partial southern Indonesia, while decreases significantly at a rate of 1.0–2.0 over the north part of Indochina and of around 3.0 over New Guinea (Fig. 3c). The R20mm trends show similar spatial distributions to those of the R10mm (Fig. 3d). The RX5day decreases significantly over the northeastern Indochina, while generally increasing over the other areas, with the most significant increasing trends of approximately 3.2 located over New Guinea (Fig. 3e). The SDII is found to increase over the whole region except for northeastern Indochina, with its significant trends of >0.2 over Kalimantan and New Guinea (Fig. 3f).

Overall, during the past several decades, areas surrounding the South China Sea tend to be drier, and the southern Philippines and Indonesia wetter. The east of Indochina and New Guinea are undergoing the most significant variation trends.

3.1.3 Spatiotemporal characteristics

Aiming at obtaining the typical spatial characteristics of extreme climate and its annual variation, the leading EOF modes and the corresponding time series are analyzed in this section. The first leading EOF mode (EOF1) of CDD accounts for 62.5% of the total variance, with negative values

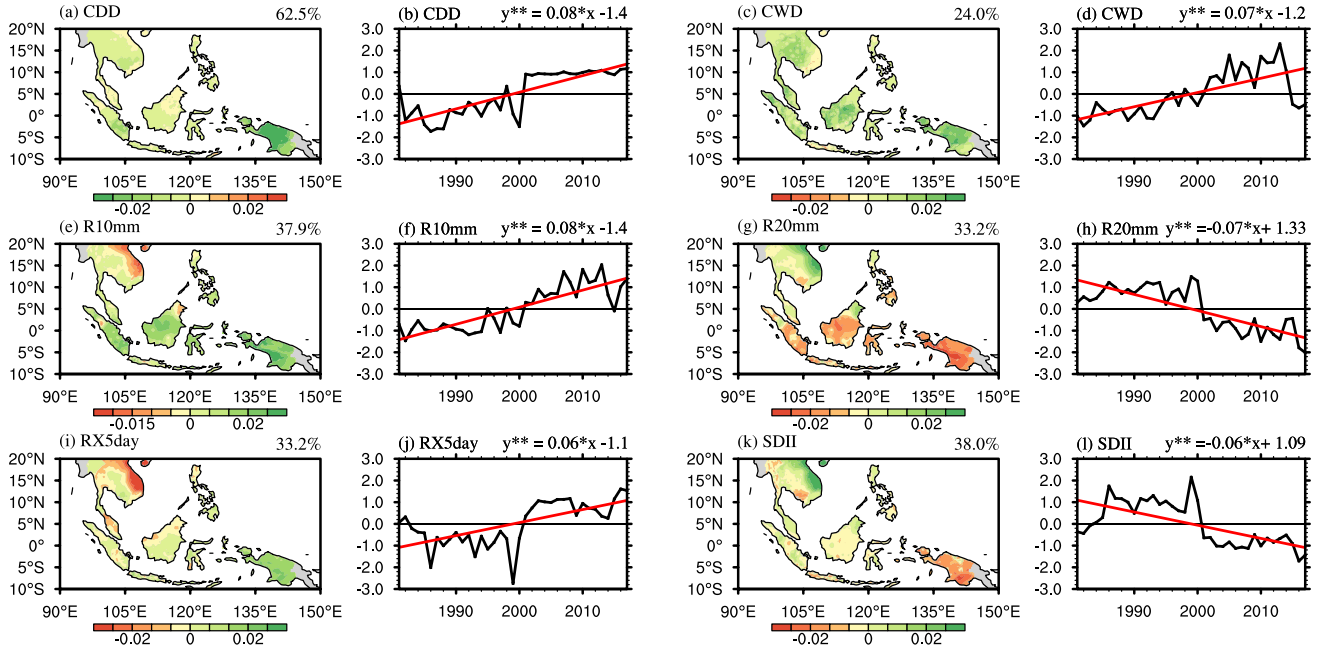

Fig. 4 Spatial patterns of the first leading EOF (EOF1) mode and the time series of the first principal component (PC1) of the **a**, **b** CDD, **c**, **d** CWD, **e**, **f** R10mm, **g**, **h** R20mm, **i**, **j** RX5day, and **k**, **l** SDII over Southeast Asia during 1981–2017. The marks of * and ** over the letter y represent that the linear regression equation is significant at 0.05 and 0.01 significance levels, respectively

mostly over the whole of Southeast Asia (Fig. 4a). The first principal component (PC1) of CDD shows a considerable increasing tendency according to the linear tendency analysis (Fig. 4b) and has experienced a significant decadal variation around 2001 according to the running *t* test (Fig. not shown). On the other hand, the EOF1 of CWD accounts for 24.0% of the total variance with positive values over most of Southeast Asia (Fig. 4c). The PC1 of the CWD increases significantly and has experienced a significant decadal variation around 2000 (Fig. 4d). With respect to the R10mm, the EOF1 accounts for 37.9% of the total variance, with positive values over Indonesia, the Philippines, and New Guinea, but negative values over the northeast of Indochina (Fig. 4e). The PC1 of R10mm increases significantly and has experienced two decadal changes around 1992 and 2005, respectively, with an average of − 0.9 during 1981–1991 and 1.1 during 2006–2017 (Fig. 4f). The EOF1 of R20mm accounts for 33.2% of the total variance with positive values over Indochina and Malaysia, while with negative values over Indonesia, the Philippines, and New Guinea (Fig. 4g). The PC1 of R20mm shows a significantly decreasing trend at a rate of 0.7 per decade (Fig. 4h) and experiences a decadal variation around 2000. The EOF1 of RX5day accounts for 33.2% of the total variance with positive values over Kalimantan, the southern Philippines, and New Guinea (Fig. 4i). The PC1 of RX5day increases significantly at a rate of 0.6 per decade with a decadal variation around 2002 (Fig. 4j). The EOF1 of SDII accounts for 38.0% of the total variance with positive values over the northeastern Indochina and Malaysia (Fig. 4k), with the corresponding PC1 significantly decreased by 0.6 per decade (Fig. 4l), experiencing two decadal variations around 1991 and 1998, with an average of 0.5 during 1981–1991, 0.9 during 1993–1997, and − 1.0 during 2005–2017.

The second leading EOF mode (EOF2) of the CDD explains 9.5% of the total variance with positive values over most of Southeast Asia (Fig. 5a). As shown in Fig. 6b, the second principal component (PC2) of the CDD shows a decreasing trend with no decadal change according to the running *t* test (Fig. 5b). The EOF2 of the CWD explains 13.2% of the total variance (Fig. 5c), with positive values over Indochina and Malaysia but negative values over Indonesia and New Guinea. The PC2 of CWD decreases significantly (Fig. 5d) with a decadal variation around 1993. The EOF2 of R10mm explains 16.7% of the total variance with negative values over most of Southeast Asia, but positive values over the south of Indochina, middle Sumatra, and New Guinea (Fig. 5e). The PC2 of R10mm shows no statistically significant trend (Fig. 5f) but experienced a significant decadal variation around 1998, with an average of − 0.1 during 1981–1997 and 0.1 during 1999–2017. The EOF2 of R20mm explains 15.3% of the total variance with positive values over Indonesia and eastern Indochina (Fig. 5g). The PC2 of R20mm shows no significant tendency (Fig. 5h) but experiences a significant decadal variation around 2000. The EOF2 of RX5day explains 12.0% of the total variance,

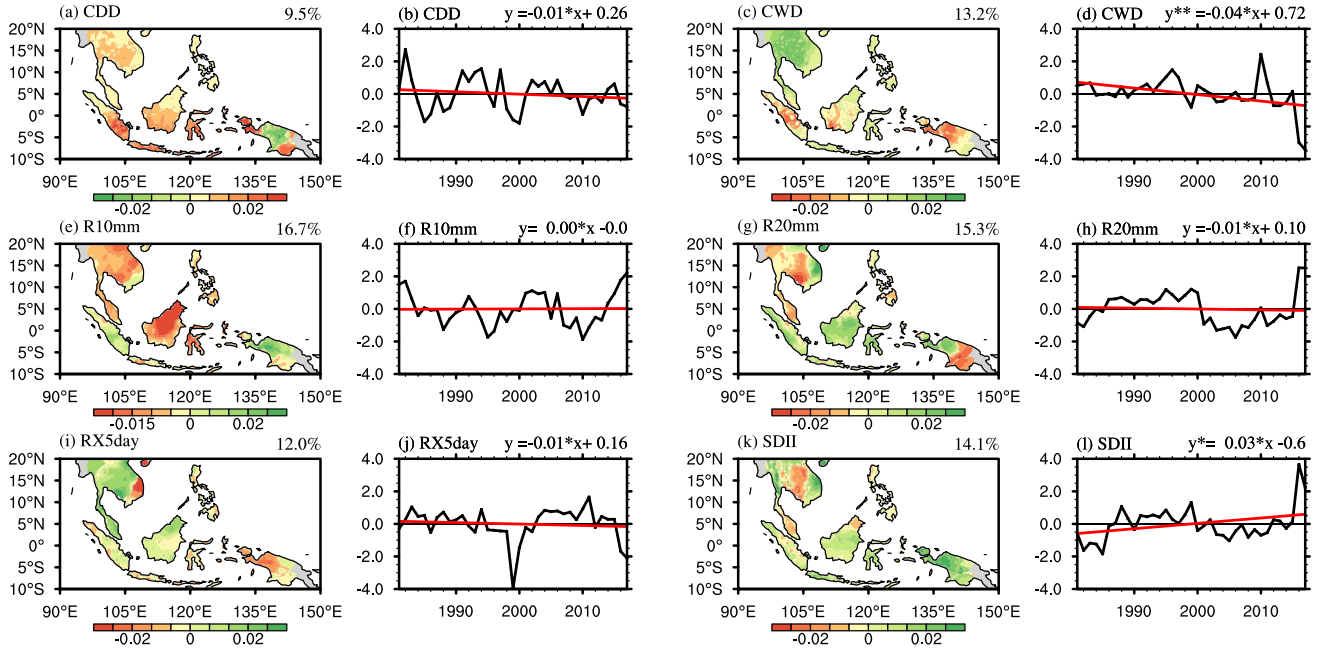

Fig. 5 Spatial patterns of the second leading EOF (EOF2) mode and the time series of the second principal component (PC2) of the **a**, **b** CDD, **c**, **d** CWD, **e**, **f** R10mm, **g**, **h** R20mm, **i**, **j** RX5day, and **k**, **l** SDII over Southeast Asia during 1981–2017. The marks of * and ** over the letter y represent that the linear regression equation is significant at 0.05 and 0.01 significance levels, respectively

with positive values over most of Indochina and Malaysia (Fig. 5i). The PC2 of RX5day shows a non-significant decrease with an average of 0.3 mm during 1981–1991, − 1.3 mm during 1996–2000, and 0.1 mm during 2007–2017 (Fig. 5j). The EOF2 of SDII explains 14.1% of the total variance with positive values over Indonesia, New Guinea, and some parts of Indochina (Fig. 5k). The PC2 of SDII increases significantly at a rate of 0.3 per decade, with a significant decadal variation around 2001 (Fig. 5l).

3.2 Temperature extremes

3.2.1 Climatological means

The spatial distributions of the climatological mean of temperature extremes in Southeast Asia during 1981–2017 are shown in Fig. 6. The distribution of temperature extreme is related to the terrain, for mountainous areas with high altitudes, such as the east of Indochina, the west of Sumatra, the central of Kalimantan, and the center of New Guinea, and the value of the temperature extreme is relatively lower than elsewhere. The minimum of daily minimum temperature (TNn) (Fig. 6a), maximum of daily minimum temperature (TNx) (Fig. 6b), minimum of daily maximum temperature (TXn) (Fig. 6c), and maximum of daily maximum temperature (TXx) (Fig. 6d) over the above-mentioned areas are lower than 16 °C, 20 °C, 22 °C, and 30 °C, while over the rest of Southeast Asia they are larger than 20 °C, 22 °C, 24 °C, and 31 °C, respectively. The areas with a relatively larger daily temperature range (DTR) are distributed in the middle of Indochina, the east of Sumatra, the central and south of Kalimantan, Sulawesi, and the center of New Guinea, with the largest values located in the northwest of Indochina (Fig. 6e).

3.2.2 Trends

The regression coefficients between time series and temperature extremes in Southeast Asia during 1981–2017 are calculated to show the variation trends (Fig. 7). The TNn increases significantly at a rate around 0.03 over most of Southeast Asia and decreases remarkably at a rate around 0.1 over the middle of New Guinea (Fig. 7a). Moreover, the trends of TNx and TXx show similar spatial distributions as that of the TNn (Fig. 7b, d). The TXn increases over the middle of Indochina and decreases in the southern Philippines (Fig. 7c). The DTR decreases notably over western Malaysia, the center of Sumatra, and western Kalimantan, and increases over northeast Indochina, the northern Philippines, and West Sulawesi (Fig. 7e).

3.2.3 Spatiotemporal characteristics

The EOF analyses are also utilized in this section to illustrate the typical spatial characteristics of temperature extreme and

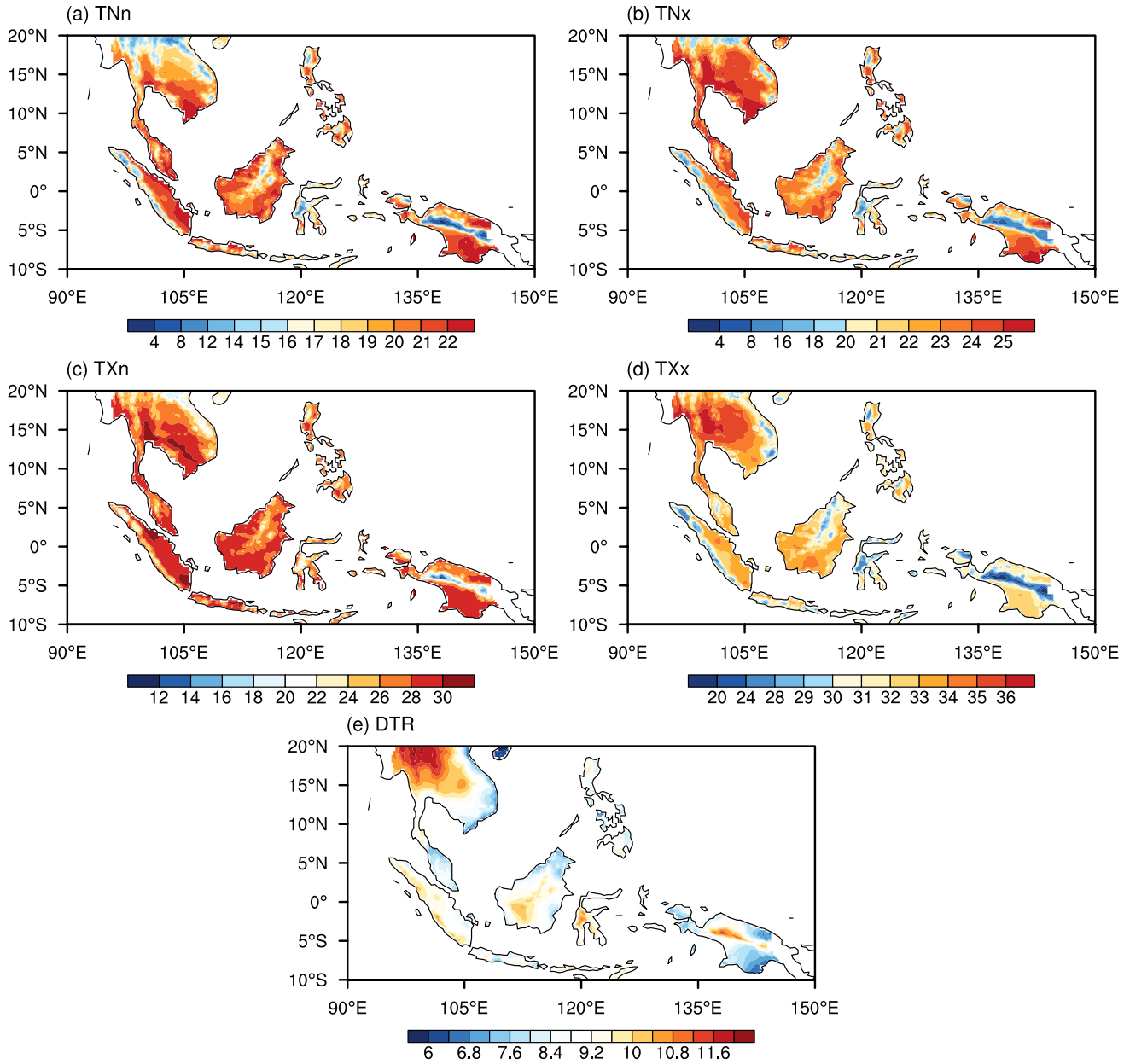

Fig. 6 Spatial distribution of the climatological mean of **a** TNn, **b** TNx, **c** TXn, **d** TXx, and **e** DTR over Southeast Asia during 1981–2017

its temporal variation. The EOF1 of TNn explains 34.1% of the total variance (Fig. 8a) with positive values over most of Southeast Asia. The PC1 of TNn increases significantly and has experienced a significant decadal variation around 2000 (Fig. 8b). The EOF1 of TNx explains 42.6% of the total variance with positive values over most of Southeast Asia (Fig. 8c). The PC1 of TNx increases and has experienced a significant decadal variation around 2001 (Fig. 8d). The EOF1 of TXn explains 23.6% of the total variance (Fig. 8e) with positive values over Indochina, eastern Malaysia, and Indonesia, and negative values over the Philippines and New Guinea. The PC1 of TXn shows no statistically significant trend but has experienced two variations around 1993 and 2005, respectively, with an average of 0.4 °C during 1981–1992 and 0.01 °C during 2006–2017 (Fig. 8f). The EOF1 of TXx explains 48.6% of the total variance (Fig. 8g) with positive values over most of Southeast Asia. The PC1 of TXx shows no statistically significant tendency (Fig. 8h) but has experienced a decadal variation around 1993. The EOF1 of DTR explains 23.0% of the total variance (Fig. 8i) with positive values over most of Southeast Asia but exhibits negative values over Malaysia, central Sumatra, and western Kalimantan, consistent with areas that decreased significantly in the linear trend of DTR. The PC1 of DTR increases

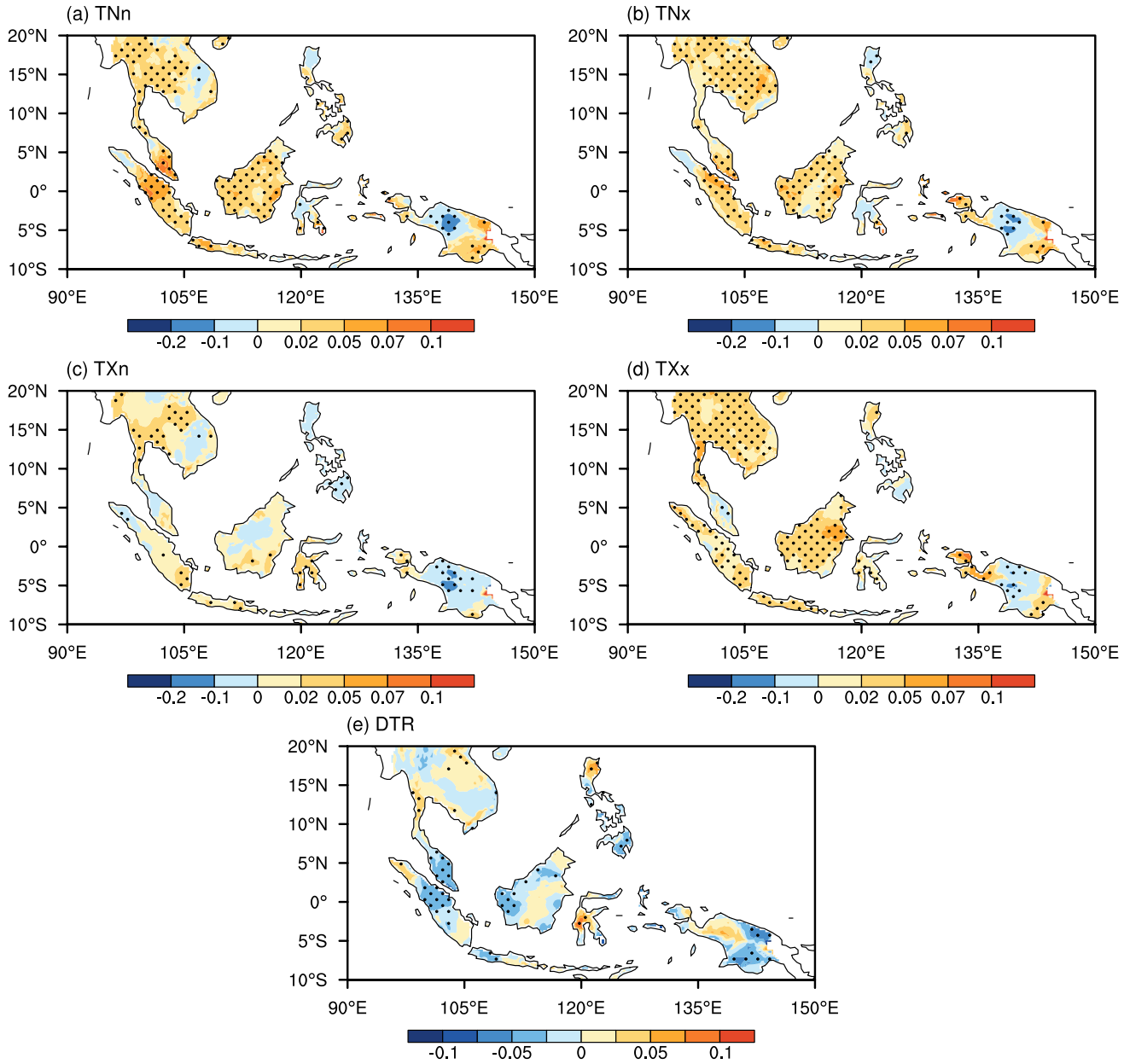

Fig. 7 The spatial trends of **a** TNn, **b** TNx, **c** TXn, **d** TXx, and **e** DTR over Southeast Asia during 1981–2017. Dotted areas are significant at the 0.01 significance level according to the Student's *t* test

significantly at a rate of 0.6 °C per decade (Fig. 8j) with a decadal variation around 1991.

The EOF2 of TNn accounts for 23.1% of the total variance with positive values over most of Southeast Asia (Fig. 9a). The PC2 of TNn increases significantly (Fig. 9b) and has experienced two decadal variations around 1991 and 2007, respectively, with an average of − 1.1 °C during 1981–1990 and 0.5 °C during 2008–2017. The EOF2 of TNx accounts for 18.0% of the total variance with negative values over most of Southeast Asia (Fig. 9c). The PC2 of TNx decreases significantly at a rate of 0.6 °C per decade (Fig. 9d) and has experienced two significantly decadal variations around 1991 and 2009, respectively, with an average of 1.1 °C during 1981–1990 and − 0.5 °C during 2010–2017. The EOF2 of TXn explains 22.3% of the total variance (Fig. 9e) with positive values over most of Southeast Asia. The PC2 of TXn (Fig. 9f) shows no significant tendency but experiences a decadal variation around 1992. The EOF2 of TXx clarifies 9.4% of the total variance (Fig. 9g) with positive values over southern Indonesia, western New Guinea, and Kalimantan, and negative values over Indochina, the Philippines, and Malaysia. The PC2 of TXx decreases significantly at

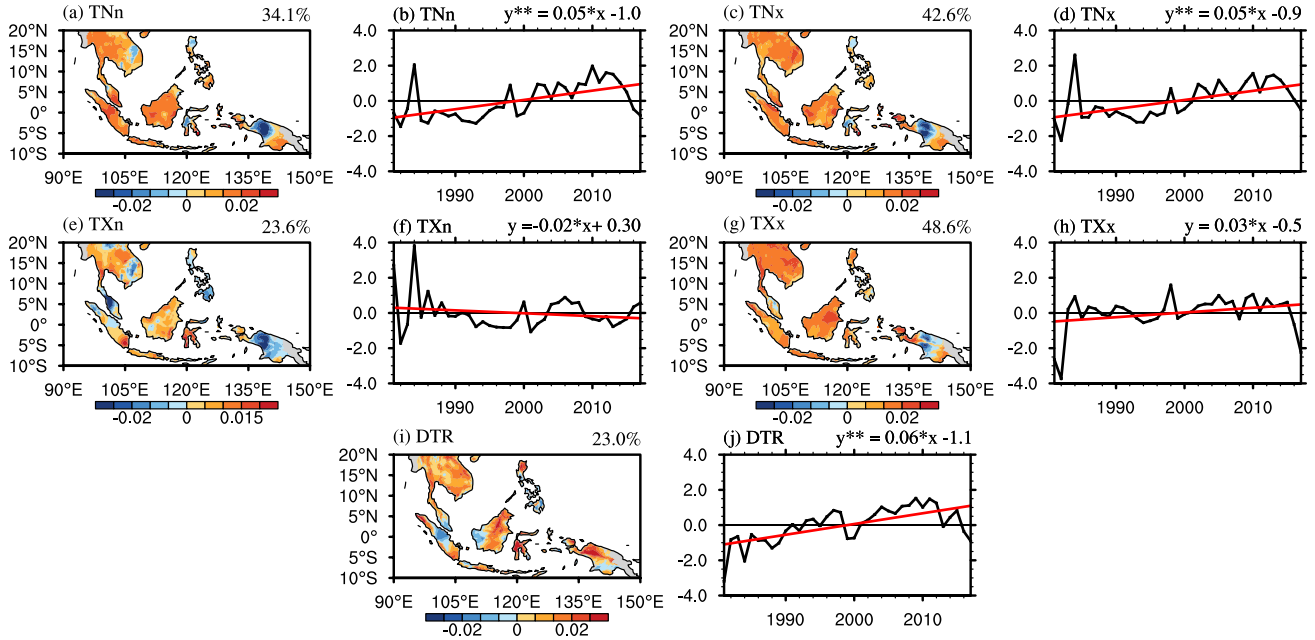

Fig. 8 Spatial patterns of the first leading EOF (EOF1) mode and the time series of the first principal component (PC1) of the **a**, **b** TNn, **c**, **d** TNx, **e**, **f** TXn, **g**, **h** TXx, and **i**, **j** DTR index over Southeast Asia during 1981–2017. The marks of * and ** over the letter y represent that the linear regression equation is significant at 0.05 and 0.01 significance levels, respectively

a rate of 0.4 °C per decade (Fig. 9h) and has experienced two decadal variations around 1993 and 2007, respectively, with an average of 0.8 °C during 1981–1992 and − 0.3 °C during 2008–2017. The EOF2 of DTR describes 20.4% of the total variance (Fig. 9i) with negative values over most of Southeast Asia. The PC2 of DTR shows no significant tendency (Fig. 9j) but has experienced a decadal variation around 1999.

In conclusion, over most of Southeast Asia, both the extremes defined by minimum temperature and those of maximum temperature show significant increasing trends. Besides, the changes in the maximum temperature extremes are smaller than those of the minimum temperature, which explains the decreasing trend of the daily temperature range.

4 Possible impacts from oceanic systems

Plenty of studies have indicated that changes in temperature and precipitation extremes are influenced by anomalous atmospheric circulations under the modulation of large-scale oceanic systems such as AMO, PDO, ENSO, and IOD (Lu et al. 2006; Yu et al. 2016; Gao et al. 2017, 2019; Shi et al. 2018). Therefore, to detect possible impacts of oceanic systems on the extremes over Southeast Asia, the correlations between the detrended PC1 and PC2 of the extremes and indices of these oceanic systems are calculated in this study and shown in Tables 2 and 3.

As a prominent sea surface temperature anomaly in the tropical Pacific Ocean, ENSO has critical impacts on atmospheric circulation and precipitation as well as extreme events throughout the world (Kenyon and Hegerl 2008; Zhou and Wu 2016; Gao et al. 2017). Specifically, the anomalous anticyclone induced by El Niño-associated warm sea surface temperature anomalies over the eastern Pacific is likely to reduce the precipitation and increase the heat risks over Southeast Asia. Almost all extreme high-temperature events over the Indochina peninsula occur in El Niño years (Thirumalai et al. 2017). Significant relationships between ENSO and extremes over Southeast Asia have been detected, especially for the precipitation extremes over the Philippines (Cheong et al. 2018; Liao et al. 2021). The Niño 3.4 index is employed here in this study to represent the ENSO intensity, which is found significantly correlated with the PC1s of CWD and R10mm in Table 2 as well as the PC2s of CDD, R10mm, DTR, TXn, and TXx in Table 3. A close relationship is hence demonstrated between ENSO and the extremes of precipitation and temperature over Southeast Asia.

AMO is a basin-wide sea surface temperature anomaly over the North Atlantic Ocean, whose phase changes could modulate the summer precipitation over Southeast Asia (Fan et al. 2019). AMO can influence the circulation background field in Southeast Asia by regulating the Eurasia teleconnection and the mid-high-latitude wave activities (Della-Marta et al. 2007; Zhou and Wu 2016). In addition, through a series of air–sea interactions, AMO regulates the Walker

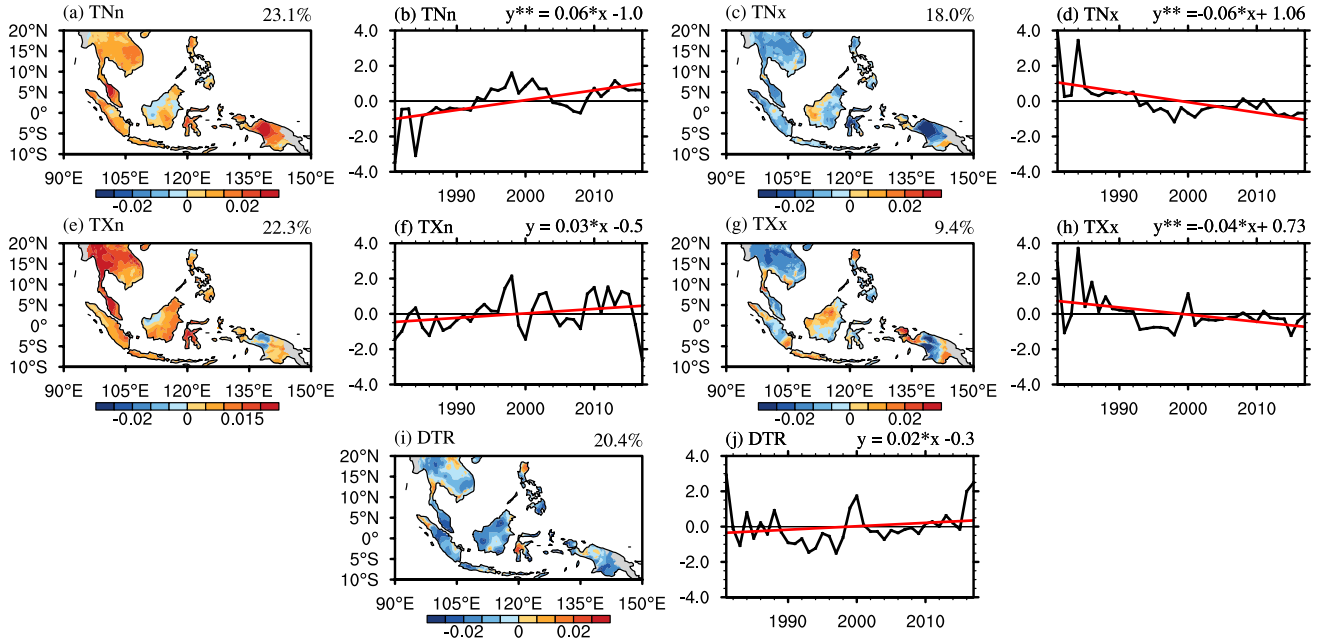

Fig. 9 Spatial patterns of the second leading EOF (EOF2) mode and the time series of the second principal component (PC2) of the **a**, **b** TNn, **c**, **d** TNx, **e**, **f** TXn, **g**, **h** TXx, and **i**, **j** DTR index over Southeast Asia during 1981–2017. The marks of * and ** over the letter y represent that the linear regression equation is significant at 0.05 and 0.01 significance levels, respectively

circulation, and therefore, induces anomalies circulation over the Pacific (Kucharski et al. 2016; Sun et al. 2017) as well as SST anomalies which influence the intensity of ENSO (Lu et al. 2008) and finally modulates the climate background over Southeast Asia. As shown in Table 2, AMO is significantly correlated with the PC1s of R10mm and R20mm indices.

As a long-lived sea surface temperature pattern over North Pacific, PDO can indirectly affect the regional climatic extremes through its influence on ENSO (Vimont et al. 2003; Higgins et al. 2007). Due to the asymmetric influence of PDO, El Niño events (Pierce et al. 2000; Wang and Liu 2016) are usually stronger in PDO warm phases than cold phases and the influences of El Niño on weather and climate in Southeast Asia are enhanced in PDO warm phases (Krishnamurthy and Krishnamurthy 2014; Fan and Fan 2017). PDO has a significant negative correlation with the PC1 of CWD, and a significant positive correlation with the PC2 of R10mm. Besides, non-significant relationship is detected between PDO and

Table 2 Correlation coefficients of the detrended PC1 and PC2 for the precipitation extreme indices and the climate indices during 1981–2017

Extreme indices	AMO	PDO	ENSO
PC1			
CWD	0.24	− 0.40*	− 0.36*
R10mm	0.40*	− 0.26	− 0.44**
R20mm	− 0.36*	− 0.05	0.07
PC2			
CDD	− 0.17	0.21	0.72**
R10mm	− 0.04	0.40*	0.45**

Only indices with at least one correlation passing the significance test are presented

*Significant at the 0.05 significance level

**Significant at the 0.01 significance level

Table 3 Correlation coefficients of the detrended PC1 and PC2 for the temperature extreme indices and the climate indices during 1981–2017

Extreme indices	ENSO	IOD	W-IO	E-IO
PC1				
TXn	− 0.29	− 0.28	− 0.36*	− 0.09
TXx	0.00	0.10	0.16	0.37*
PC2				
DTR	− 0.43**	− 0.27	− 0.21	− 0.01
TNn	0.17	0.24	0.38*	0.20
TNx	− 0.24	− 0.27	− 0.40*	− 0.16
TXn	0.33*	0.32*	0.32*	0.17
TXx	− 0.42**	− 0.29	− 0.43**	− 0.11

Only indices with at least one correlation passing the significance test are presented

*Significant at the 0.05 significance level

**Significant at the 0.01 significance level

the temperature extremes, reflecting the greater impact of PDO on precipitation extremes than temperature.

Illustrating the sea surface temperature gradient between the W-IO and the E-IO, IOD has significant impacts on local temperature and precipitation over Southeast Asia. It is pointed out that the IOD would influence the climate globally (Saji and Yamagata 2003), and positive phase of IOD often appears with El Niño, increasing the number of warm nights over Southeast Asia (Allan et al. 2001; Saji and Yamagata 2003; Behera et al. 2005; Chen et al. 2018). In this study, the correlations between extreme indices and IOD, as well as the W-IO and the E-IO are presented in Tables 2 and 3. Indian Ocean SST anomalies show significant impacts on temperature extremes (Table 3), consistent with previous investigations (Cheong et al. 2018).

To make further investigation on the relationship between the ocean systems and the extremes, the spatial distribution of correlation coefficients between the principal components (PCs) of EOF modes and the detrended SST as well as lower level circulations and geopotential height are analyzed (Figs. 10, 11). To be noticed, only the PCs with correlations significant at the 0.01 significance level (Tables 2, 3) are presented. In details, the PCs meeting the above requirement are the PC1 of R10mm, PC2 of CDD, PC2 of R10mm, PC2 of DTR, and PC2 of TXx. As shown in Figs. 10 and 11, correlations between SST and the PCs all show similar patterns over the tropical Pacific area: precipitation and temperature extremes accompanied by ENSO-like SST anomalies over the tropical Pacific, geopotential height anomalies located over the marine-time continent, and zonal wind anomalies over Southeast Asia, indicating that the anomalous Walker circulation induced by ENSO is critical for the variation of extremes. To be noticed, the PC1 of R10mm also shows a significant relationship with the SST over North Atlantic (Fig. 10a and Table 2). Previous studies found that the warmer (colder) Atlantic alters the zonal circulation, resulting in anomalous ascending (descending) motion in the Atlantic and descending (ascending) motion in the central Pacific, inducing anomalous pressure and wind anomalies

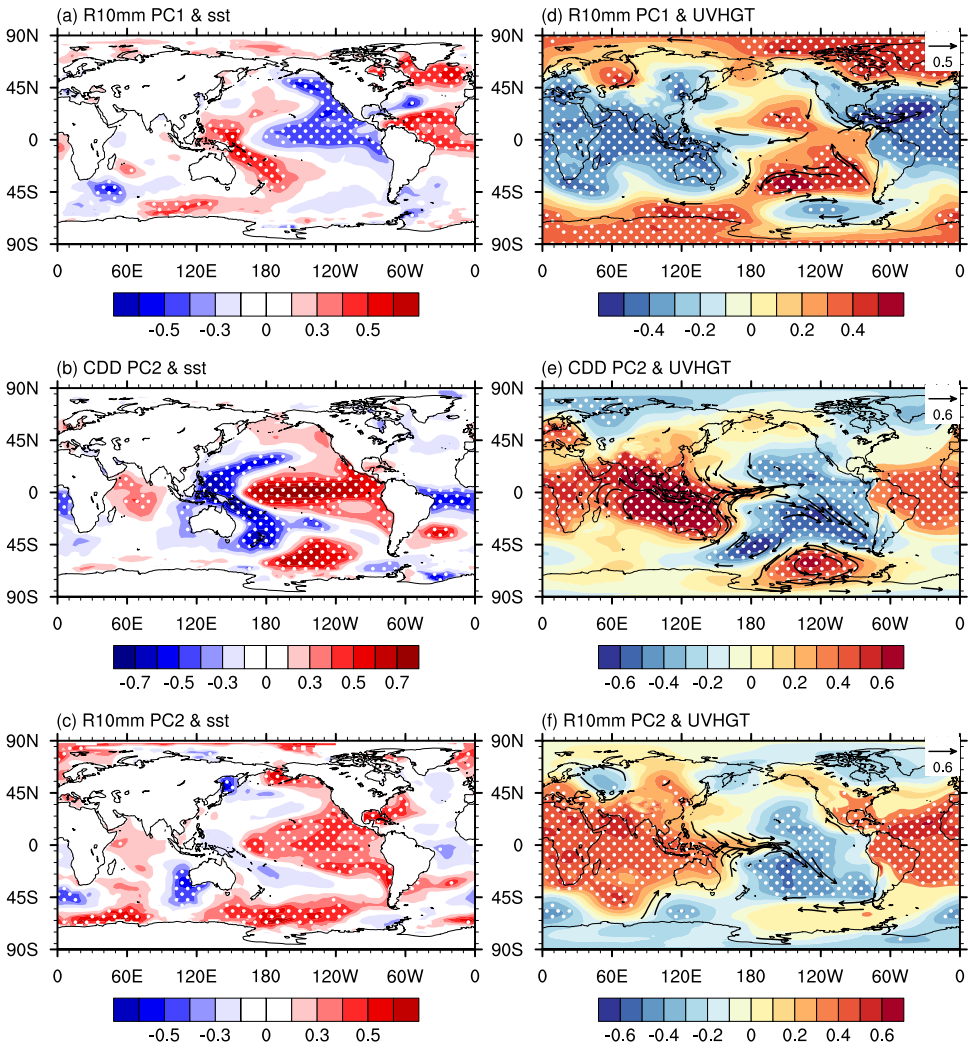

Fig. 10 The correlation coefficient between SST and the **a** PC1 of R10mm, **b** PC2 of CDD, **c** PC2 of R10mm, and the correlation coefficients between 850 hPa geopotential height (shaded), 850 hPa wind (vector) and the **d** PC1 of R10mm, **e** PC2 of CDD, and **f** PC2 of R10mm during 1981–2017. Dotted areas and plotted wind vectors are significant at the 0.05 significance level according to the Student's *t* test

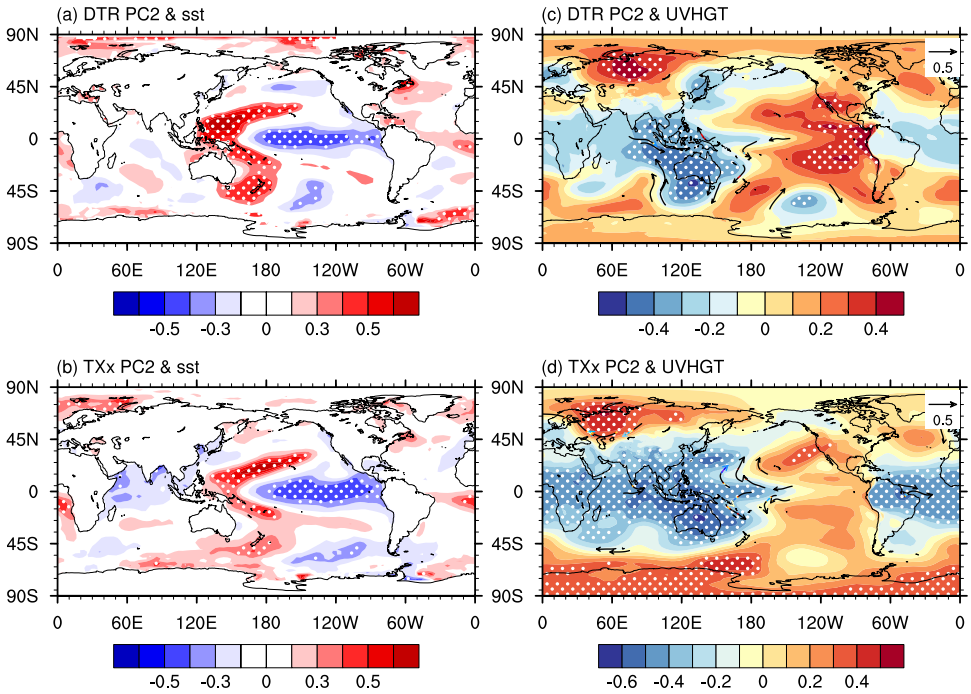

Fig. 11 The correlation coefficient between SST and the **a** PC2 of DTR, **b** PC2 of TXx and the correlation coefficients between 850 hPa geopotential height (shaded), 850 hPa wind (vector) and the **c** PC2 of DTR and **d** PC2 of TXx during 1981–2017. Dotted areas and plotted wind vectors are significant at the 0.05 significance level according to the Student's *t* test

over the South China Sea through a series of air–sea interactions (McGregor et al. 2014; Kucharski et al. 2016). Besides, AMO would excite Eurasia teleconnection anomaly through modulating Rossby wave activity, resulting in an anomalous vertical motion, lower level zonal wind, and water vapor transport over the Indo-China Peninsula (Gui et al. 2021). As shown in Fig. 10d, the significant correlations between R10mm and the geopotential height and lower troposphere wind over Eurasia and central North Pacific indicate the possible influence from AMO. The T-N wave activity flux (Takaya and Nakamura 2001) anomalies and geopotential height anomalies at 700 hPa level under the influence of the AMO (Fig. S1) indicate that positive (negative) phase of the AMO tends to stimulate eastward propagating Rossby wave anomalies from North Atlantic to East Asia, resulting in positive (negative) geopotential height anomalies over the north (south) part of Southeast Asia. For negative (positive) geopotential height anomalies at lower level troposphere being advantageous (disadvantages) to upward motion and precipitation, the above-mentioned relationship might explain why positive AMO favors less (more) precipitation extremes over the north (south) part of Southeast Asia (Table 2 and Fig. 4).

In conclusion, the variations of wet extremes are correlated with the AMO, PDO, and ENSO, while dry extremes are only significantly related to ENSO. Extreme high temperatures exhibit a considerable relationship with ENSO and IOD at interannual time-scale, while low temperatures present significant correlations with IOD. Notably, IOD is characterized by more obvious influences on the temperature extremes than the precipitation extremes over Southeast Asia, among which the equatorial western Indian Ocean has a greater contribution. Moreover, AMO and PDO tend to modulate the precipitation extremes rather than the temperature extremes.

5 Conclusion and discussion

The climatological means, trends and spatial–temporal variations of the precipitation and temperature extremes during 1981–2017 over Southeast Asia are analyzed in this study, as well as the possible influences from oceanic systems. Results are concluded as follows:

1. Spatial distributions of the climatological means of extreme indices indicate that New Guinea and the western Indochina are characterized by generally more intense precipitation extremes than Kalimantan and the eastern Indochina. The distributions of temperature extremes are found to be related to the terrain. Over the higher altitude mountainous areas such as the east of Indochina, the west of Sumatra, the central of Kalimantan, and the center of New Guinea, the temperature extremes are relatively lower than elsewhere.
2. From 1981 to 2017, areas surrounding the South China Sea tend to be drier while the southern Philippines and Indonesia tend to be wetter. Significant trends are detected over the east of Indochina and New Guinea. Besides, extremes defined by temperatures of daily max-

imum and minimum show significant increasing trends in most of Southeast Asia. The changes in the maximum temperature extremes over most of Southeast Asia are smaller than those of the minimum temperature, being consistent with the decreasing trend of the daily temperature range.

3. The typical modes of both precipitation and temperature extremes show uneven spatial distributions according to the EOF analysis, and the corresponding PCs exhibit different temporal variations. The PC1 and PC2 of extremes mainly present decadal and interannual variations, respectively. The PC1s of most precipitation extremes show significant increasing trends and significant decadal variations around the late 1990s. According to the correlations between oceanic systems and the PC1s of the extreme EOFs, the modulation of decadal variations could be associated with the AMO and PDO. Moreover, most of the PC2s of the low-temperature extremes exhibit significant relationships with Indian Ocean for interannual variations, whereas high-temperature extremes are in relationship with ENSO.

Studies indicate that global warming does affect climate extremes in Southeast Asia. Most of the extreme precipitation and temperature indices increase significantly over Indochina Peninsula and maritime continent in a warming world (Ge et al. 2019). In the dry season, DTR decreases in the central areas of Indochina and increases in other areas, while increasing significantly over most of Southeast Asia in the wet season (Zhu et al. 2020). Besides, the declining Arctic sea ice shows significant influence on hot and drought over the East Asia (Gao et al. 2015; Li et al. 2018; Ji and Fan 2019). The variation of Northern Hemisphere sea ice extent is in close relationship with the PC2 of temperature extremes such as the TXx (Tables S1 and S2) and the related mechanisms are to be explore in the future work. Moreover, the El Niño and Indian Ocean Dipole events will occur more frequently with the continuous global warming, which in turn brings larger variability over the climate in Southeast Asia (Zheng et al. 2013; Chen et al. 2014; Cai et al. 2014, 2018; Geng et al. 2019). Therefore, how the extremes change in a global warming world would be further analyzed.

Supplementary Information The online version contains supplementary material available at https://doi.org/10.1007/s00703-022-00913-6.

Acknowledgements This work is jointly supported by Grants from the National Natural Science Foundation of China (Grants 42025502; 42105030; 42005015), the Natural Science Foundation of the Jiangsu Higher Education Institutions of China (21KJB170005) and the Natural Science Foundation of Jiangsu Province (BK20200814). We also thank the support from the Startup Foundation for Introducing Talent of NUIST.

Data availability Raw observations data were provided by the Southeast Asia Climate Assessment and Dataset project at http://sacad.database.bmkg.go.id/. Monthly Sea Surface Temperature (SST) data are derived from U.S. National Oceanic and Atmospheric Administration Extended Reconstructed SST V5 at https://psl.noaa.gov/data/gridded/data.noaa.ersst.v5.html. Geopotential height and wind datasets are obtained from European Centre for Medium-Range Weather Forecasts (ECMWF) ERA5 at https://doi.org/10.24381/cds.6860a573. The monthly series of the large-scale oceanic systems indices are obtained from the U.S. National Oceanic and Atmospheric Administration Physical Sciences Laboratory at https://psl.noaa.gov.

References

Alexander LV, Zhang XB, Peterson TC et al (2006) Global observed changes in daily climate extremes of temperature and precipitation. J Geophys Res Atmos 111:1042–1063. https://doi.org/10.1029/2005JD006290

Allan RJ, Chambers D, Drosdowsky W et al (2001) Is there an Indian Ocean Dipole and is it independent of the El Niño–Southern Oscillation? CLIVAR Exch 6:18–22

Behera SK, Luo JJ, Masson S et al (2005) A CGCM study on the interaction between IOD and ENSO. J Clim 19:1688–1705. https://doi.org/10.1175/JCLI3797.1

Brohan P, Kennedy JJ, Harris I, Tett SFB, Jones P (2006) Uncertainty estimates in regional and global observed temperature changes: a new dataset from 1850. J Geophys Res 111:D12106. https://doi.org/10.1029/2005JD006548

Caesar J, Alexander LV, Trewin B et al (2011) Changes in temperature and precipitation extremes over the Indo-Pacific region from 1971 to 2005. Int J Climatol 31:791–801. https://doi.org/10.1002/joc.2118

Cai W, Santoso A, Wang GJ et al (2014) Increased frequency of extreme Indian Ocean Dipole events due to greenhouse warming. Nature 510:254–258. https://doi.org/10.1038/nature13327

Cai W, Wang G, Dewitte B et al (2018) Increased variability of eastern Pacific El Niño under greenhouse warming. Nature 564:201–206. https://doi.org/10.1038/s41586-018-0776-9

Chen ZS, Wen ZP, Wu RG et al (2014) Influence of two types of El Niños on the East Asian climate during boreal summer: a numerical study. Clim Dyn 43:469–481. https://doi.org/10.1007/s00382-013-1943-1

Chen J, Wang X, Zhou W et al (2018) Unusual rainfall in southern China in decaying August during extreme El Niño 2015/16: role of the western Indian Ocean and north tropical Atlantic SST. J Clim 31:7019–7034. https://doi.org/10.1175/JCLI-D-17-0827.1

Cheong WK, Timbal B, Golding N, Sirabaha S, Kwan KF, Cinco TA, Archevarahuprok B, Vo VH, Gunawan D, Han S (2018) Observed and modelled temperature and precipitation extremes over Southeast Asia from 1972 to 2010. Int J Climatol 38:3013–3027. https://doi.org/10.1002/joc.5479

Della-Marta PM, Luterbacher J, Weissenfluh H et al (2007) Summer heat waves over western Europe 1880–2003, their relationship to large-scale forcings and predictability. Clim Dyn 29:251–275. https://doi.org/10.1007/s00382-007-0233-1

Donat MG, Alexander LV, Yang H et al (2013) Updated analyses of temperature and precipitation extreme indices since the beginning of the twentieth century: the HadEX2 dataset. J Geophys Res Atmos 118:2098–2118. https://doi.org/10.1002/jgrd.50150

Endo N, Matsumoto J, Lwin T (2009) Trends in precipitation extremes over Southeast Asia. Sola 5:168–171. https://doi.org/10.2151/sola.2009-043

Fan Y, Fan K (2017) Pacific decadal oscillation and the decadal change in the intensity of the interannual variability of the South China Sea summer monsoon. Atmos Ocean Sci Lett 10:162–167. https://doi.org/10.1080/16742834.2016.1256189

Fan K, Xu ZQ, Tian BQ (2014) Has the intensity of the interannual variability in summer rainfall over South China remarkably increased? Meteorol Atmos Phys 124:23–32. https://doi.org/10.1007/s00703-013-0301-5

Fan Y, Fan K, Zhu X et al (2019) El Niño-related summer precipitation anomalies in Southeast Asia modulated by the Atlantic multidecadal oscillation. J Clim 32:7971–7987. https://doi.org/10.1175/JCLI-D-19-0049.1

Fischer EM, Knutti R (2015) Anthropogenic contribution to global occurrence of heavy-precipitation and high-temperature extremes. Nat Clim Chang 5:560–564. https://doi.org/10.1038/nclimate2617

Gao Y, Sun J, Li F et al (2015) Arctic sea ice and Eurasian climate: a review. Adv Atmos Sci 32:92–114

Gao T, Wang HJ, Zhou T (2017) Changes of extreme precipitation and nonlinear influence of climate variables over monsoon region in China. Atmos Res 197:379–389. https://doi.org/10.1016/j.atmosres.2017.07.017

Gao M, Yang J, Gong D et al (2019) Footprints of Atlantic multidecadal oscillation in the low-frequency variation of extreme high temperature in the Northern Hemisphere. J Clim 32:791–802. https://doi.org/10.1175/JCLI-D-18-0446.1

Ge F, Zhu SP, Peng T et al (2019) Risks of precipitation extremes over southeast asia: does 1.5 °C or 2 °C global warming make a difference. Environ Res Lett 14:044015. https://doi.org/10.1088/1748-9326/aaff7e

Ge F, Zhu S, Sielmann F et al (2021) Precipitation over Indochina during the monsoon transition: modulation by Indian Ocean and ENSO regimes. Clim Dyn 57:2491–2504. https://doi.org/10.1007/s00382-021-05817-6

Geng T, Yang Y, Wu L (2019) On the mechanisms of Pacific decadal oscillation modulation in a warming climate. J Clim 32:1443–1459. https://doi.org/10.1175/JCLI-D-18-0337.1

Gui S, Yang R, Cao J, Tan S, Janjai S, Dong Z (2021) The influence of the Atlantic multidecadal oscillation on the interdecadal variability of winter precipitation in the Greater Mekong Subregion. Int J Climatol 41(10):5072–5083

Hersbach H, Bell B, Berrisford P et al (2019) ERA5 monthly averaged data on pressure levels from 1979 to present. Copernicus Climate Change Service (C3S) Climate Data Store (CDS). https://doi.org/10.24381/cds.6860a573

Higgins RW, Silva VBS, Shi W et al (2007) Relationships between climate variability and fluctuations in daily precipitation over the United States. J Clim 20:3561–3579. https://doi.org/10.1175/JCLI4196.1

Huang B, Thorne PW, Vf B et al (2017) Extended reconstructed sea surface temperature version 5 (ERSSTv5), upgrades, validations, and intercomparisons. J Clim 30:8179–8205. https://doi.org/10.1175/JCLI-D-16-0836.1

IPCC (2013) Climate change 2013: the physical science basis. Contribution of Working Group I to the Fifth Assessment Report of the Intergovernmental Panel on Climate Change. Cambridge University Press, Cambridge, United Kingdom and New York, NY, USA 1535

Ji L, Fan K (2019) Climate prediction of dust weather frequency over northern China based on sea-ice cover and vegetation variability. Clim Dyn 53:687–705

Kenyon J, Hegerl GC (2008) Influence of modes of climate variability on global temperature extremes. J Clim 21:3872–3889. https://doi.org/10.1175/2008JCLI2125.1

Krishnamurthy L, Krishnamurthy V (2014) Influence of PDO on South Asian summer monsoon and monsoon–ENSO relation. Clim Dyn 42(9–10):2397–2410. https://doi.org/10.1007/s00382-013-1856-z

Kucharski F, Ikram F, Molteni F et al (2016) Atlantic forcing of Pacific decadal variability. Clim Dyn 46:2337–2351. https://doi.org/10.1007/s00382-015-2705-z

Li W, Yuan C (2019) Decadal variations of winter extreme cold days in northern China. J Geosci Environ Prot 7:241–250. https://doi.org/10.4236/gep.2019.78018

Li H, Chen H, Wang H et al (2018) Can Barents Sea ice decline in spring enhance summer hot drought events over northeastern China? J Clim 31:4705–4725

Liao W, Fan Y, Zhu S et al (2021) Monthly variations of the winter precipitation over the Philippines during the mature phase of eastern pacific El Niño. Front Earth Sci 8:625455. https://doi.org/10.3389/FEART.2020.625455

Lu R, Dong B, Ding H (2006) Impact of the Atlantic multidecadal oscillation on the Asian summer monsoon. Geophys Res Lett 33:L24701. https://doi.org/10.1029/2006GL027655

Lu R, Chen W, Dong B (2008) How does a weakened Atlantic thermohaline circulation lead to an intensification of the ENSO–South Asian summer monsoon interaction? Geophys Res Lett 35:L08706. https://doi.org/10.1029/2008GL033394

Manton MJ, Della-Marta PM, Haylock MR et al (2001) Trends in extreme daily rainfall and temperature in Southeast Asia and the South Pacific: 1961–1998. Int J Climatol 21:269–284. https://doi.org/10.1002/joc.610

McGregor S, Timmermann A, Stuecker MF et al (2014) Recent Walker circulation strengthening and Pacific cooling amplified by Atlantic warming. Nat Clim Change 4:888–892. https://doi.org/10.1038/NCLIMATE2330

Nicholls N, Baek HJ, Gosai A et al (2005) The El Niño–southern oscillation and daily temperature extremes in East Asia and the West Pacific. Geophys Res Lett 32:L16714. https://doi.org/10.1029/2005GL022621

Pierce DW, Barnett TP, Latif M (2000) Connections between the Pacific Ocean tropics and midlatitudes on decadal timescales. J Clim 13:1173–1194. https://doi.org/10.1175/1520-0442(2000)013%3c1173:CBTPOT%3e2.0.CO;2

Qian C, Zhang X (2019) Changes in temperature seasonality in China: Human influences and internal variability. J Clim 32:6237–6249. https://doi.org/10.1175/JCLI-D-19-0081.1

Saji NH, Yamagata T (2003) Possible impacts of Indian Ocean Dipole mode events on global climate. Clim Res 25:151–169. https://doi.org/10.3354/cr025151

Schleussner CF, Lissner TK, Fischer EM et al (2016) Differential climate impacts for policy-relevant limits to global warming: the case of 1.5 °C and 2 °C. Earth Syst Dyn 7:327–351. https://doi.org/10.5194/esd-7-327-2016

Shi J, Cui L, Wen K et al (2018) Trends in the consecutive days of temperature and precipitation extremes in China during 1961–2015. Environ Res 161:381–391. https://doi.org/10.1016/j.envres.2017.11.037

Si D, Ding Y (2016) Oceanic forcings of the interdecadal variability in East Asian summer rainfall. J Clim 29:7633–7649. https://doi.org/10.1175/JCLI-D-15-0792.1

Sun C, Kucharski F, Li J et al (2017) Western tropical Pacific multidecadal variability forced by the Atlantic multidecadal oscillation. Nat Commun 8:15998. https://doi.org/10.1038/ncomms15998

Takaya K, Nakamura H (2001) A formulation of a phase-independent wave-activity flux for stationary and migratory quasigeostrophic eddies on a zonally varying basic flow. J Atmos Sci 58:608–627. https://doi.org/10.1175/1520-0469(2001)058%3c0608:AFOAPI%3e2.0.CO;2

Thirumalai K, DiNezio PN, Okumura Y et al (2017) Extreme temperatures in Southeast Asia caused by El Niño and worsened by global warming. Nat Commun 8:1–8. https://doi.org/10.1038/ncomms15531

Van den Besselaar EJM, van der Schrier G, Cornes RC et al (2017) SA-OBS: a daily gridded surface temperature and precipitation dataset for Southeast Asia. J Clim 30:5151–5165. https://doi.org/10.1175/JCLI-D-16-0575.1

Vimont DJ, Wallace JM, Battisti DS (2003) The seasonal footprinting mechanism in the Pacific: implications for ENSO. J Clim 16:2668–2675. https://doi.org/10.1175/1520-0442(2003)016%3c2668:tsfmit%3e2.0.co;2

Wang XD, Liu HL (2016) PDO modulation of ENSO effect on tropical cyclone rapid intensification in the western North Pacific. Clim Dyn 46(1–2):15–28. https://doi.org/10.1007/s00382-015-2563-8

Yu L, Zhong S, Pei L et al (2016) Contribution of large-scale circulation anomalies to changes in extreme precipitation frequency in the United States. Environ Res Lett 11:044003. https://doi.org/10.1088/1748-9326/11/4/044003

Zander KK, Richerzhagen C, Garnett ST (2019) Human mobility intentions in response to heat in urban South East Asia. Glob Environ Change 56:18–28. https://doi.org/10.1016/j.gloenvcha.2019.03.004

Zheng XT, Xie SP, Du Y et al (2013) Indian Ocean dipole response to global warming in the CMIP5 multimodel ensemble. J Clim 26:6067–6080. https://doi.org/10.1175/JCLI-D-12-00638.1

Zhou Y, Wu Z (2016) Possible impacts of mega-El Niño/Southern Oscillation and Atlantic multidecadal oscillation on Eurasian heatwave frequency variability. Q J R Meteorol Soc 142:1647–1661. https://doi.org/10.1002/qj.2759

Zhu S, Ge F, Fan Y et al (2020) Conspicuous temperature extremes over Southeast Asia: seasonal variations under 1.5 °C and 2 °C global warming. Clim Change 160:343–360. https://doi.org/10.1007/s10584-019-02640-1